I. Introduction

SINCE the pioneering work of Brown and Roshko[1] and Winant and Browand[2], it has been known that large-scale vortical structures play a pivotal role in the dynamics of the free shear layer flows. Therefore, any attempt of active control of such flows has been focused on the manipulation of the dynamics of these large coherent structures. It has been shown for the past three decades that the vortical structures evolving in the free shear layer and separated flows can be manipulated, at least within a limited band of wavelengths, through the introduction of controlled disturbances at the flow boundary (e.g., Ho and Huerre[3]). Hence, the traditional approach to the alteration of these flows has focused on the modification of entrainment of inviscid fluid through global, two-dimensional (or axisymmetric) instability modes (e.g., Roberts and Roshko[4]) and on the initiation of low-wavenumber, three-dimensional motions (e.g., Breidenthal[5], Nygaard and Glezer[6]). The first work to characterize the effect of introduction of controlled disturbances on shear layers used mechanical devices for actuators applied to a two-stream shear layer. Both Ho and Huang[7] and Oster and Wygnanski[8] used this approach to manipulate the instability modes of the flow. Working in a water tunnel, Ho and Huang[7] used valves to input velocity perturbations and were able to control the spreading rate of a two-stream shear layer by manipulating vortex merging. Oster and Wygnanski[8] used an oscillating flap to inhibit the growth of a two-stream shear layer. They found that small amplitude oscillations (low-level forcing) increase the spreading rate of the shear layer and larger amplitude forcing causes the layer to resonate, having vortical structures which do not interact with one another, eliminating the lateral growth of the layer. Reisenthel, Nagib, and Koga[9] used periodic oscillations of a mechanical flap to control reattachment length of the separated flow in a single stream shear layer. Other methods for actuating the flow include self-oscillating wire in the flow (Vandsburger and Ding[10]) and acoustic speakers (Huang and Ho[11], Ho et al[12], Chun and Sung[13], and Chun, Lee, and Sung[14]). Such actuation produced increased mixing in the near field and enhanced entrainment by affecting the large structures created by the natural frequency of the layer. In a numerical study, Kaiktsis and Monkewitz[15] employed a combination of suction on the step face and blowing downstream of the step to destabilize the separated flow. They concluded that their strategy works well for more-easily simulated laminar flows but uncertainty is expressed concerning the application to the more relevant case of turbulent flow. The review paper by Ho and Huerre[3] provides an extensive overview of two-stream shear layers and applicable low-frequency forcing methods.

High frequency actuation has been extensively applied in flow control applications where it was sought to effectively decouple the actuation input from the fundamental unstable frequencies of the base flow. Examples include control of the aerodynamic performance of bluff and streamlined bodies (e.g., Amitay et al.[16], Honohan, et al.[17]) and enhanced mixing in a plane (e.g., Wiltse and Glezer[18,19] and Smith and Glezer[20]) and axisymmetric (e.g., Davis and Glezer[21]) jets. These flow control applications were enabled by the introduction and characterization of synthetic jet actuators (Smith and Glezer[22] and Glezer and Amitay[23]). These previous investigations have demonstrated that high-frequency actuation has a profound impact on evolution of free- and wall-bounded turbulent shear flows even though the actuation is introduced locally at scales that are typically an order of magnitude smaller than the naturally dominant scales of the base flow. However, as demonstrated by Wiltze and Glezer[18], the excitation of discrete wave numbers within the dissipation range of the baseline flow can lead to strong coupling between small- and large-scale motions. Vukasinovic, Lucas, and Glezer[24] showed that direct high-frequency actuation has a profound effect on the evolution of both large- and small-scale motions within the shear layer by inducing a localized increase in small-scale dissipation. They effected the high-frequency actuation to the active flow control of a single-stream shear layer via an array of synthetic jet actuators. This work has demonstrated that despite adding turbulent kinetic energy to the flow, the actuation leads to an initial increase in turbulent dissipation that is followed by suppression of turbulent production within the layer, ultimately producing an overall reduction in turbulent kinetic energy relative to the baseline (unforced) flow.

Although the high-frequency actuators operate nominally at the frequencies that are an order of magnitude higher than the naturally-evolving frequencies in the flow, they can be also used to manipulate fluid motions that are comparable to the "natural" frequencies. Large-scale motions are introduced by low-frequency amplitude-modulation of the high-frequency signal. Wiltse and Glezer[18] first demonstrated experimentally that the spectral sidebands of the time harmonic, high-frequency actuation waveform that are introduced through amplitude modulation induce coherent motions at the modulation frequency. This approach adds large-scale motions to the directly induced small-scale motions in the flow and has been used in other flow control applications to the shear flows (Davis and Glezer[21], Smith and Glezer[20]). Vukasinovic, Lucas and Glezer[24] showed that the ensuing large vortical structures in the flow scale with the modulation frequency and that their formation distance increases with the decrease in the modulation frequency. This conclusion led to the further investigation of the dynamics of formation of these large structures, and Vukasinovic, Lucas, and Glezer[25] postulated that these large-scale coherent

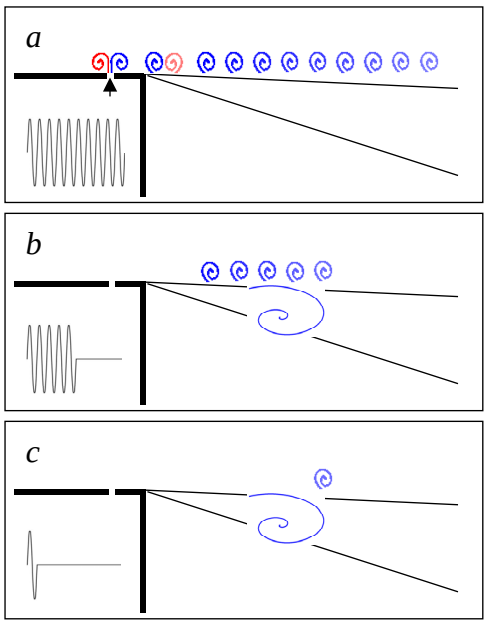

Figure 1. Schematics of the shear layer forced by the high-frequency signal in continuous (*a*), burst (*b*), and pulse-like (*c*) mode using direct high-frequency actuation.

motions (at scales comparable to the cross-stream width of the layer) are induced indirectly by the transients associated with onset and termination of the actuation cycle. Concomitant excitation of both small and large scales leads to enhanced mixing through direct enhancement of the small-scale motions and augmented entrainment by the induced large-scales. As a result, the turbulent kinetic energy (especially within the large scales) as well as the cross stream spreading of the layer are significantly enhanced. In the absence of the transients that lead to the formation of the large scale structures, continuous high-frequency actuation results in stabilization of the base flow.

Since the formation of a large coherent structure depends only on the transient disruption of the boundary layer (BL) vorticity, Vukasinovic et al[25] further showed that a train of large coherent structures can be sustained simply by periodic pulsing of the shear layer at the desired rate using a single high-frequency actuation cycle. This opened the possibility of indirect low-frequency actuation of the shear layer with the sole application of high-frequency pulsed forcing. Therefore, nominally three modes of control can be effected using the direct high-frequency actuation: continuous, burst, and pulse-like, as shown schematically in Figure 1. The major focus of the present work is on the single-period (quasi-pulsed) actuation, although some aspects of both burst and continuous actuations are presented as a complement or contrast to the single-period fluidic control. It should be noted that a quasi-pulsed flow control using synthetic actuators bears a lot similarities to combustion-driven fluidic control[26,27], which is inherently of pulsed nature. Current work also builds on the previous findings and further explores the dynamics of the large-scale structures that are formed in the burst and pulsed mode. Burst mode essentially allows a ratio of high-frequency vortices to a single large structure to be adjusted, while there is only a single high-frequency vortex per single large structure in the actuation mode shown in Figure 1*c*. As these burst or pulsed events can be repeated at any desired instants in time, they can be applied either at the fixed rate or randomly. Therefore, they can be induced "at will" at periodic or any other prescribed aperiodic rate, thus forming the "coded" shear layer structure that carries the corresponding "windows" of high and low optical transmittance.

The present work is motivated by the previous investigations of the direct high-frequency forcing effect on turbulent shear layers, operated in either continuous, burst, or pulsed mode[24,25] and, as noted above, by recent evidence of the flow stabilization by the continuous high-frequency actuation. This work is focused on the transient, pulse-like excitation of large coherent structures in the shear flows, without or with the concomitant direct small-scale excitation. It investigates all three modes of actuation (cf. Figure 1) as ultimately, by increasing a number of subsequent pulses, the burst mode of actuation transitions to the continuous mode. The experimental setup and procedures are described in Section II. Section III characterizes the baseline (unforced) flow. Comparison between the direct low-frequency actuation and pulsed high-frequency actuation is presented in Section IV. Section V describes different burst-mode actuations including the transition to continuous actuation. Stabilizing effect of continuous actuation is demonstrated in Section VI. Finally, conclusions of this investigation are discussed in Section VII.

II. Experimental Setup and Procedures

This experimental work is conducted in a low-speed, closed return wind tunnel that is specifically designed for high-resolution PIV measurements. The test section has transparent walls on three sides and measures $25.4 \times 40.6 \times 132.1$ cm. The tunnel has no screens and is equipped with a minimal number of honeycomb sections to avoid PIV seeding blockage and accumulation. Nonetheless, the free stream turbulence intensity is not compromised and is measured to be less than 0.5% over the entire range of tunnel speeds. Figure 2 shows a schematic diagram of the flow configuration. The shear layer is generated by the flow separation off the edge of a backward-facing step, which is built in the top wall of the test section and the flow evolves in canonical single-stream shear layer. The step

spans the full width of the test section and its height relative to the top wall of the test section is H = 50.8 mm. It should be noted that in spite of the actual step orientation, all results are presented in a flipped field of view.

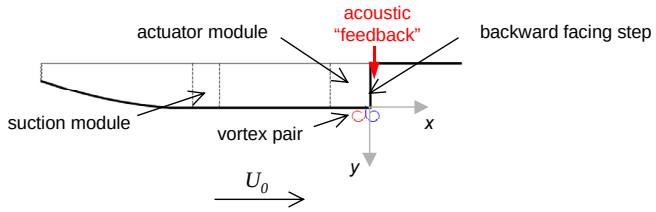

Figure 2. Schematics of the flow configuration.

A six-module synthetic jet actuator is integrated into the step surface. The orifice of each individually-controlled module measures 0.38 × 18.3 mm and the spanwise spacing between adjacent orifices is 1.9 mm (the actuators span about 95% of the step). The actuator orifices are 8 mm (21 orifice widths) upstream of the step edge and the jets issue normal to the step surface. Each module is calibrated outside of the test section by measuring cross stream velocity distributions over the exit orifice using hot wire anemometry (HWA). A movable miniature pressure probe is used for assessing the module performance *in-situ* between the runs. Besides the actuator module, the step is equipped with the acoustic source, which exit slit is built in the top wall along the corner that meets the vertical step wall (Figure 2). Acoustic slit has 0.8 mm width and spans across 80% of the test section width. The input to the actuators is a time-harmonic signal at St = 7.36 for the given flow speed. Such input signal is modified to result in transitory one, three, five, and seven periods of excitation at St = 7.36 that are repeated at f = 200 Hz repetition rate, which corresponds to St = 0.74. Continuous actuation at St = 7.36 is also applied to contrast the transitory modes of actuation. Acoustic actuation of the shear layer is always effected by time-harmonic sinusoidal signal at St = 0.74. The boundary layer over the step surface is tripped well upstream of the edge (using a 1 mm diameter trip wire) and the flow over the actuators is turbulent.

The flow characterization in spatial domain spanning $-0.5 < x/H < 2.5$ and $-0.5 < y/H < 0.5$ or $0 < x/H < 2$ and $-0.25 < y/H < 0.25$ (in the vertical, x-y plane) is done using high-resolution particle image velocimetry (PIV) having a nominal imaging resolution of 27 μm/pixel. The PIV measurements are taken over eleven or four partially overlapping windows and the CCD camera and part of the laser-sheet optics are mounted on computer-controlled traverse mechanisms. Spectral analysis of the flow is based on a single-sensor hot-wire anemometry. For that purpose, spectral measurements are done across shear layer at the x/H = 0, 0.5, 1, 1.5, and 2 downstream locations using the computer-controlled traverse that carries a miniature HW probe.

III. The Baseline Flow

The unforced (baseline) flow is characterized in the full spatial domain using the PIV measurements. The ensemble-averaged flow field is shown in Figure 3. Figure 3*a* shows raster plot of the mean vorticity field with equidistant mean velocity profiles. As expected, the mean flow evolves slowly in the downstream direction, and the presence of the wall and finite step height affect the velocity profiles as weak, recirculating flow is formed below the low stream edge of the shear layer. As the boundary layer decays and the single-stream shear layer is formed, there is an asymmetry in its cross stream spreading owing to the entrainment on the nearly-stagnant (wall) side, and as a result, the shear layer spreads more on this side. Figure 3*b* shows a raster plot of the corresponding 2-D estimate of the turbulent kinetic energy (TKE) of the baseline flow. First, a narrow zone of high TKE is marked immediately downstream from the step edge, resulting from the decaying boundary layer. Once the boundary layer dissipates, there is a drop in absolute level of TKE. Further downstream, TKE increases with the shear layer formation, as the energy of the entrained motions is transferred towards the small scales. The highest TKE levels are consistently in the shear layer core, with the highest absolute level measured at the downstream end of the domain.

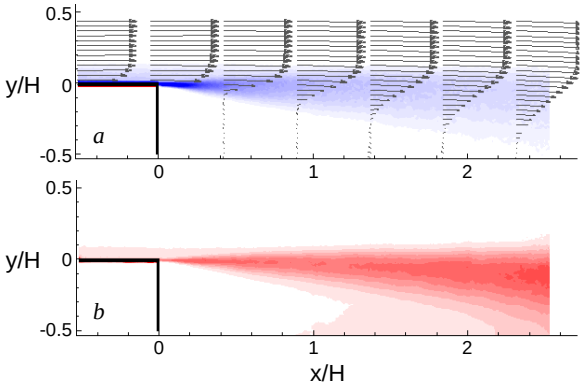

Figure 3. Raster plots of spanwise vorticity field with equidistant velocity profiles (*a*) and a 2-D estimate of the TKE *k* (*b*) of the baseline flow. Vorticity ζ_z (s^{-1}) contour levels: -4000 4000. TKE (m^2/s^2) contour levels: -5 5.

Further characterization of the baseline flow is focused on the boundary layer analysis at the step edge (x/H = 0), as some of the BL parameters (e.g., momentum thickness θ and Re_θ) are known to govern evolution of the ensuing shear layer. BL mean velocity profile $\overline{U}/u_\tau$ is measured by the constant temperature miniature hot wire probe and is

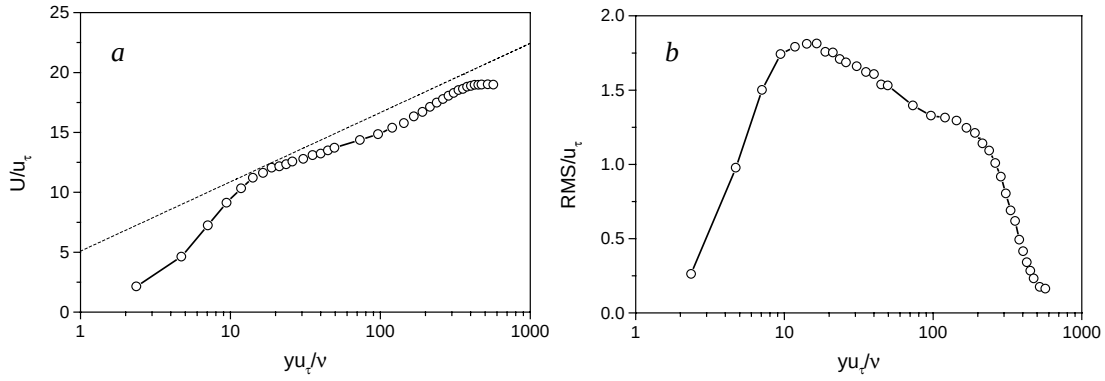

Figure 4. Mean velocity (*a*) and the profile of RMS velocity fluctuations (*b*) for the boundary layer of the baseline flow at *x*/*H* = 0. The log-law $\overline{U}/u_\tau = 2.51\ln(yu_\tau/\nu)+5.1$ is shown as a reference (---).

shown in Figure 4*a* in wall coordinate $y^+ = yu_\tau/\nu$. The measured profile somewhat departs from the fully turbulent one, which is manifested by a slight undershooting of the log-law profile $\overline{U}/u_\tau = 2.51\ln(yu_\tau/\nu)+5.1$, which can be attributed to the trip-assisted transition to turbulence and the upstream feedback from the recirculating flow beneath the shear layer. Figure 4*b* shows the corresponding BL RMS velocity fluctuations in wall coordinate, which follows the expected turbulent BL profile, having the peak velocity fluctuations between y^+ = 10 – 20. Derived BL parameters that are of interest for the resulting shear layer are: momentum thickness θ = 0.9 mm, shape factor h = 1.39, and Reynolds number based on momentum thickness and half the free stream velocity Re_θ = 401. Based on θ and Re_θ, the most amplified frequency of the baseline flow is estimated to be f_n = 243 Hz (St_θ = 0.032)[3].

IV. Transitory and Time-Harmonic Actuation

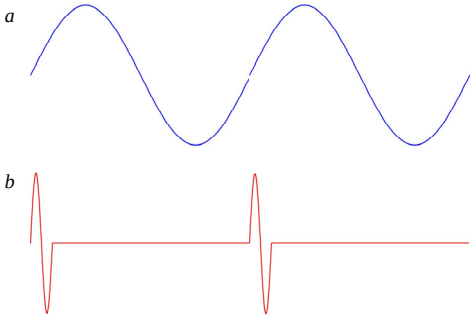

Figure 5. Schematics of the continuous acoustic signal (*a*) and a single-period, transitory signal (*b*).

Vukasinovic, Lucas, and Glezer[25] demonstrated excitation of a single coherent structure in a shear layer with each transient modulation of the nominally continuous actuation signal. The present study focuses on a comparison between two shear layers with prescribed scale (frequency) of the coherent structure. In the first case, this structure is induced by time-harmonic acoustic actuation at the prescribed frequency *f*, as shown schematically in Figure 2. In the second case, analogous coherent structures are induced using the transient injection of a single vortex pair generated at 2000 Hz with the repetition rate that matches the prescribed frequency *f*. Coherent structure frequency (scale) is selected such that $f_n/2 < f$ = 200 Hz $< f_n$, where f_n is the most amplified frequency at *x*/*H* = 0 (Section III). Therefore, Strouhal number based on the step height for the time-harmonic acoustic excitation is *St* = 0.74, while the transient actuation is an order of magnitude higher *St* = 7.36. Two actuation signals are schematically shown in Figure 5.

As seen in Figure 2, acoustic excitation, meant to emulate feedback to the shear layer most receptive region, originates at the corner formed by vertical and horizontal walls beneath the step edge. Transitory actuation is effected through the flow boundary layer upstream from the step edge (*x*/*H* = -0.16). To match the relevant actuation amplitudes and compare these two excitations, it is assumed that the energy of the dominant input "disturbance" at *f* should be matched in both cases. This is done by the spectral characterization of the actuated shear layer at the most receptive zone - shear layer origination. The measurement location is selected to be just downstream from the step edge (*x*/*H* = 0.004). Measured cross-stream profiles of spectral energy at prescribed frequency *f* = 200 Hz are shown in Figure 6 for two matched excitation cases, along with the corresponding profile for the baseline (unforced) flow. Two excitation cases are found to be matched when integrated energy profiles are equal. Although the total energy is matched there are differences in individual profiles. Both profiles have nearly identical absolute maximum close to *y* = 0. However, profile of the transitory actuation exhibits secondary peak that corresponds to the passage of a single small-scale vortex. Furthermore, it appears that the transitory excitation

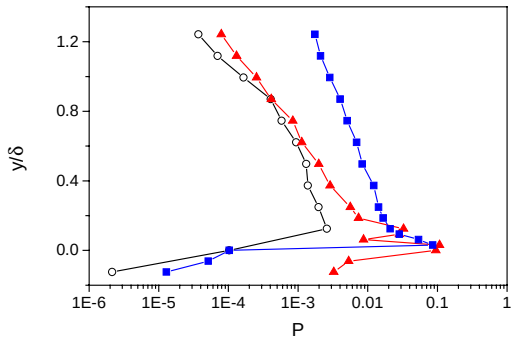

Figure 6. Spectral energy profiles at f = 200 Hz of the flow at x/H = 0.004 for the baseline (∘), continuous acoustic (■, St = 0.74) and a single-period (▲, St = 7.36) actuation at the 200 Hz repetition rate.

results in higher energy content at the low-speed edge (y < 0), while the opposite is true towards the free-stream edge. Both forced flows exhibit order of magnitude higher absolute spectral peaks compared to the spectral energy profile of the baseline case.

Once parameters for the two excitation cases are selected, global effect of the actuation on the mean flow is checked at the most receptive region of the shear layer, measured again immediately downstream from the step edge (x/H = 0.004). Mean velocity and RMS velocity fluctuations are measured using the HWA and Figure 7 shows the baseline (unforced), acoustically- and transitory-forced profiles. There is virtually no difference in the mean velocity profiles among all cases, while the same conclusion holds for the RMS profiles of the baseline and acoustically-forced flow. RMS profile of the transitory-forced flow follows the other two with only one exception that the peak is reduced 5-10% relative to the other two. Such suppression is a signature of the boundary layer forced by the high-frequency actuation, and it is interesting to note that there is still a notable peak reduction in spite of the single-period "pulsing" instead of continuous high-frequency actuation. Overall, despite a considerable addition of energy at the prescribed frequency f = 200 Hz when compared to the baseline flow, there is just a minute modification of the *mean* flow at the shear layer onset in either of the forced cases.

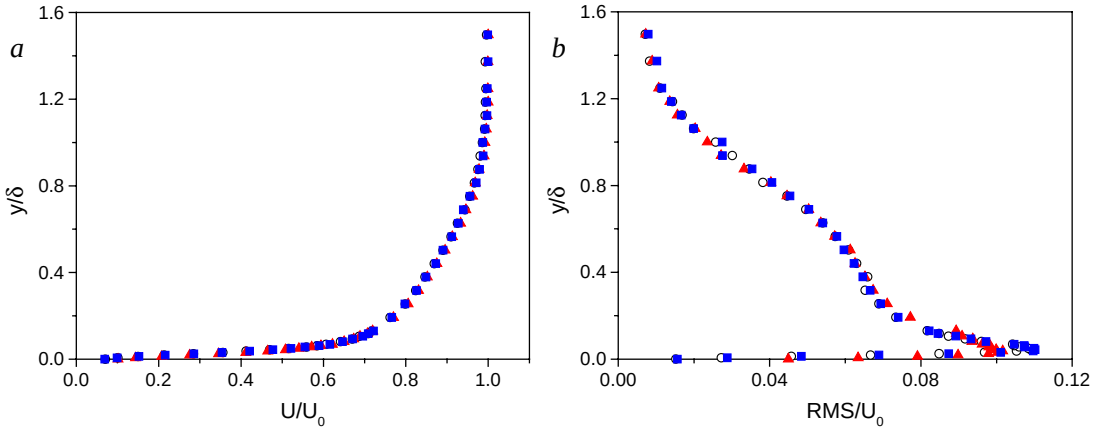

Figure 7. Mean velocity (*a*) and the profile of RMS velocity fluctuations (*b*) of the flow at x/H = 0.004 for the baseline (∘), continuous acoustic (■, St = 0.74) and a single-period (▲, St = 7.36) actuation at the 200 Hz repetition rate.

In order to elucidate induced coherent structures and their flow signatures in the acoustically-forced flow, PIV measurements are done phase-locked with the excitation signal fed to the speaker. Measured velocity vector field $\boldsymbol{V}(t)$ at the phase ϕ is originally decomposed into the coherent $\boldsymbol{V}_C(\phi)$ and incoherent (random) $\boldsymbol{v}'(t)$ parts. A representative phase-frozen flow structure is shown in Figure 8*a* where raster plot of vorticity is shown for an arbitrary phase ϕ = 160°. Three coherent structures are visible at this phase, namely at x/H = 0.55, 1.2, and 2. The corresponding contour plot of the total turbulent kinetic energy k is shown in Figure 8*b*. It is seen that the zones of highest k are tied to the coherent structures, with increasing levels of k in the downstream direction. To obtain coherent velocity fluctuations that contribute to the coherent part of k, $\boldsymbol{V}_C(\phi)$ is further decomposed into the mean velocity $\overline{\boldsymbol{V}}$ and coherent fluctuation $\boldsymbol{v}_C'(\phi)$. After that, contribution of both coherent and incoherent (random) velocity fluctuations to total k is calculated and shown in Figures 8*c*–*d*, respectively. Figure 8*c* clearly isolates zones of high coherent turbulent kinetic energy, which appear tied to both leading and trailing edges of each coherent structure. Having the coherent contribution subtracted from the total k, it is seen in Figure 8*d* that the incoherent part is more uniformly distributed throughout the shear layer, with a magnitude increase in the downstream direction. It is also seen that coherent part of k plays significant role in the initial, formation part of the shear layer, while incoherent part dominates further downstream, as major transfer of energy towards the small scales is spatially

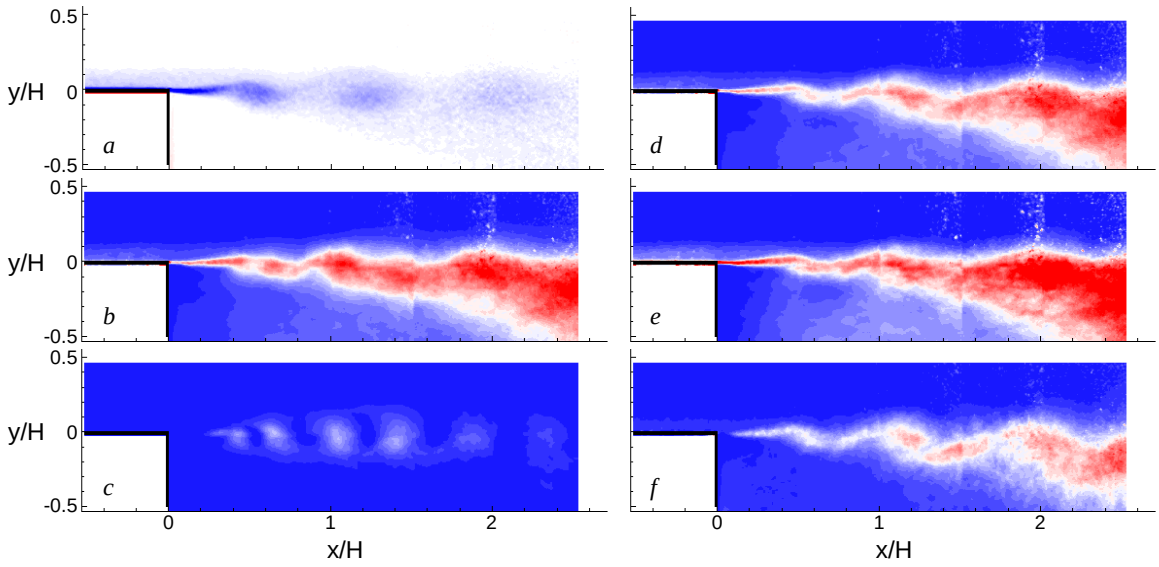

Figure 8. Phase-averaged (ϕ = 160°) raster plots of: vorticity (*a*), a 2-D estimate of the total turbulent kinetic energy *k* (*b*), coherent (*c*) and incoherent (*d*) components of *k*, and incoherent components of streamwise (*e*) and cross-stream (*f*) normal stresses. Shear layer is forced by the continuous acoustic actuation (*St* = 0.74). Vorticity levels are same as in Fig. 3. TKE (m^2/s^2) contour levels: 0 5

delayed and preceded by entrainment. Contributions of streamwise and cross-stream velocity fluctuations to the incoherent part of *k* are further examined through the contour plots of normal stresses in the streamwise and cross-stream direction, which are shown in Figures 8*e–f*, respectively. It is clear that normal stress component in the streamwise direction dominates as a consequence of the dominant flow direction. The cross-stream component is more tied to the coherent structures. Large entrainment of fluid in the cross-stream direction is facilitated via motions of the coherent structures, and as the outer fluid gets engulfed into the structure, it continues to transfer energy to smaller scales, thereby generating high turbulent intensities in its core. Therefore, high intensities of normal stress in the cross-stream direction is spatially delayed.

Analogous to the coherent structure analysis of the acoustically-forced flow, the representative characteristics of the transitory-forced shear layer are shown in Figure 9 for the phase ϕ = 160°. Raster plot of vorticity is shown in

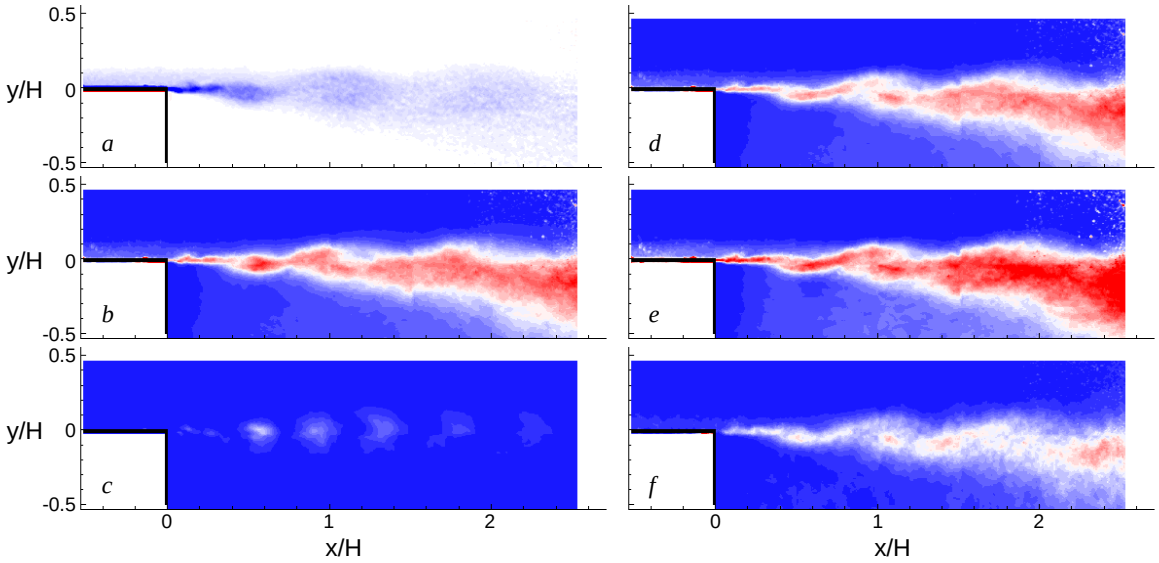

Figure 9. Phase-averaged (ϕ = 160°) raster plots of: vorticity (*a*), a 2-D estimate of the total turbulent kinetic energy *k* (*b*), coherent (*c*) and incoherent (*d*) components of *k*, and incoherent components of streamwise (*e*) and cross-stream (*f*) normal stresses. Shear layer is forced by a single-period actuation (*St* = 7.36) at the 200 Hz repetition rate. Contour levels are same as in Fig. 8.

Figure 9*a* and three coherent structures are visible again, only slightly more diffused than their acoustically-forced counterparts (Figure 8*a*). Closer look at the plot also reveals the presence of a single high-frequency vortex (x/H = 0.2) with the clockwise (CW) sense of vorticity. Its CCW pair dissipates shortly after being injected into the boundary layer flow. The remaining two coherent structures resulted from the previous two vortex pairs injected into the flow. More diffused coherent structures are characterized with less intense levels of k, its components and stresses (Figures 9b-f, respectively), although the flow structure is almost identical to the acoustically-forced flow. Such attenuation in magnitude can be a consequence of the selected criterion for a match of two cases - as described above, integrated energy at f = 200 Hz is matched for both cases. However, as acoustic forcing is imposed at the boundary of recirculating region, its actual amplitude has to be set higher than of the pulsed forcing, which is directly carried into the shear layer (Figure 2). The other possibility for attenuation of energy magnitudes may be due to "disruptive" interaction of the single high frequency vortex and the initial coherent structure roll-up. Further support for this interpretation may be found in the plot of coherent component of k (Figure 9*c*). If compared to its "acoustical" counterpart (Figure 8*c*), it is seen that the initial zone of high coherent energy at the trailing edge of the coherent structure is suppressed ostensibly due to the interaction with the CW vortex. Once disrupted, such coherent vortex would never gain entrainment commensurate to its uninterrupted counterpart. In general, these examples show remarkable similarity in the instantaneous flow structure between time-harmonic and transitory-forced shear layers.

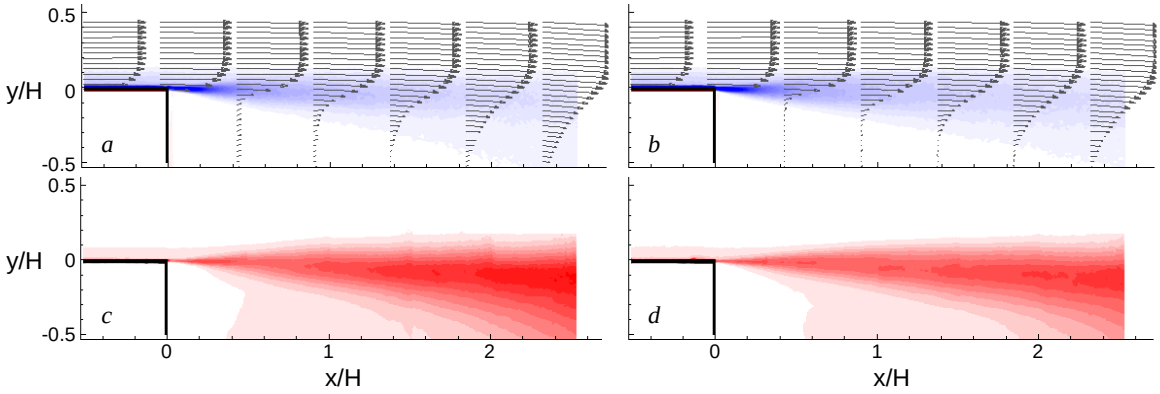

Figure 10. Raster plots of the spanwise vorticity fields with overlaid velocity profiles (*a*, *b*) and the corresponding 2-D estimates of the turbulent kinetic energy *k* (*c*, *d*) for the flow actuated by a continuous acoustic signal at *St* = 0.74 (*a*, *c*) and by a single-period signal at *St* = 7.36 and the 200 Hz repetition rate (*b*, *d*). Contour levels are same as in Fig.3.

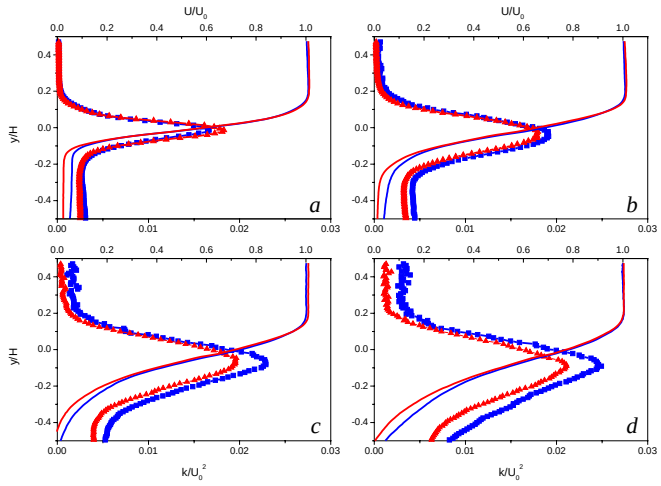

Figure 11. Profiles of the mean *U* velocity component and TKE *k* at *x*/*H* = 0.5 (*a*), 1.0 (*b*), 1.5 (*c*), and 2.0 (*d*) for the shear layer forced by a single-period actuation (, ▲, *St* = 7.36) at the 200 Hz repetition rate and by continuous acoustic actuation (, ■, *St* = 0.74).

Having the similarity of instant flow structure in both actuation cases shown, it is expected that the resulting mean flow features are also similar. Ensemble-averaged spanwise vorticity fields with equidistant mean velocity profiles are shown in Figures 10*a* and 10*b*, for the acoustically- and transitory-forced shear layers, respectively. It should be noted that, as expected, somewhat larger spreading of the shear layer is measured for the acoustically-forced flow, which also has stronger recirculating flow that is a consequence of the location of the acoustic source and stronger amplitude of the forcing compared to the transitory case. If compared to the mean baseline flow (Figure 3*a*), both forced flows spread much more towards the low-speed side, as a direct consequence of the enhanced entrainment via induced coherent structures. The corresponding raster plots of a 2-D estimate of turbulent kinetic energy k for the acoustically- and transitory-forced shear layers are shown in Figures 10*c* and 10*d*, respectively. Again, as expected, higher

energy content is measured for the "acoustic" case. Also, both raster plots of k show high levels in the narrow region that corresponds to the decaying boundary layer, with re-emergence of the highest levels of k after the formation and dissipation of large coherent structures towards the downstream end of the measurement domain. If compared to the baseline flow (Figure 3*b*), both forced cases demonstrate significant increase in both the absolute magnitude of k and spatial spreading of zones of increased k levels. Further comparison between acoustically- and transitory-forced shear layers is shown in Figure 11, where mean streamwise velocity and k profiles are plotted at x/H = 0.5, 1, 1.5, and 2. At x/H = 0.5 (Figure 11*a*), mean velocity profiles are overlapped over the shear layer, while, although still weak, velocity is the recirculating flow is two times higher in acoustically-forced flow. This is a consequence of the acoustic source location and its interaction with the shear layer through the recirculating region. TKE profiles exhibit a narrow peak within the shear layer in both cases, with close overlap, except that transitory-forced flow has slightly higher peak magnitude. By the next downstream location (x/H = 1, Figure 11*b*), shear layer spreads similarly in both cases, with stronger recirculating flow in the acoustically-forced flow. The shear layer spreading is also evident in spreading of the TKE profiles, which is more pronounced at the low-speed edge. Both TKE profiles are similar in shape, with the distinction that acoustically-forced peak magnitude now becomes stronger than in its transitory counterpart. Also, stronger recirculating flow starts to induce higher TKE levels in the recirculating region. At x/H = 1.5 (Figure 11*c*), more pronounced spreading of the acoustically-forced shear layer is seen, with continued spreading of the TKE profiles. Both TKE profiles are still similar in shape, having peak magnitudes shifted towards the low-speed side, with higher levels of TKE now pronounced in acoustically-forced flow over the whole cross-section. Finally, the noted trend continues in the profiles shown at the last location x/H = 2 (Figure 11*d*). The acoustically-forced shear layer spreads more, with a further increase in TKE magnitude.

Comparison between two actuation approaches is further done in spectral domain using the single sensor HWA. Power spectra for both actuations are derived from the measured velocity fluctuations across the shear layer at four downstream locations x/H = 0.5, 1, 1.5, and 2. Four power spectra for each actuation are shown in Figure 12, derived for the measurements at the cross-stream location $y|_{0.5}$ where local mean velocity is half the free stream velocity. At x/H = 0.5 (Figure 12*a*), both flows exhibit strong peaks at the prescribed frequency f = 200 Hz of the coherent structure indicating strong coherent motions. Furthermore, energy content of these motions is stronger in the transitory- than in the acoustically-forced flow. Also, weak motions corresponding to two higher harmonics are present in the flow in both cases, which can be a consequence of not pure-tone input from both sources. Besides the distinct peaks, broadband energy distribution is identical is either case. It is interesting that energy content at f = 200 Hz decreases in both cases at x/H = 1 (Figure 12*b*), with second harmonics dissipated and first harmonics diminished but still present in the flow. There is somewhat increased energy level across the large scales in the transitory-forced flow, while the small-scale energy distribution is still identical. Also, evolving turbulent flow in the downstream direction due to continuous transfer of energy from the engulfed surrounding fluid is marked by the formed inertial region in the power spectra. Although suppressed at the previous measured location, strong coherent motions reappear at x/H = 1.5 (Figure 12*c*). The first harmonic is almost completely suppressed, and distribution of energy across the scales is comparable in either actuation. As the flow further evolves, inertial region widens and spreads towards the smaller scales as a consequence of decrease of scales at which transfer of energy ultimately ends in dissipation. At the last measurement location x/H = 2 (Figure 12*d*), only strong distinct peaks at the dominant coherent motion are present in both flows and inertial region is spread further onto the small scales. It should be also noted that subsequent to the roll-up of induced coherent motions, broadband energy of the large scales also increases in the downstream direction (e.g., compare Figures 12*a* and 12*d*). Overall, there is a big similarity in spectral energy distribution

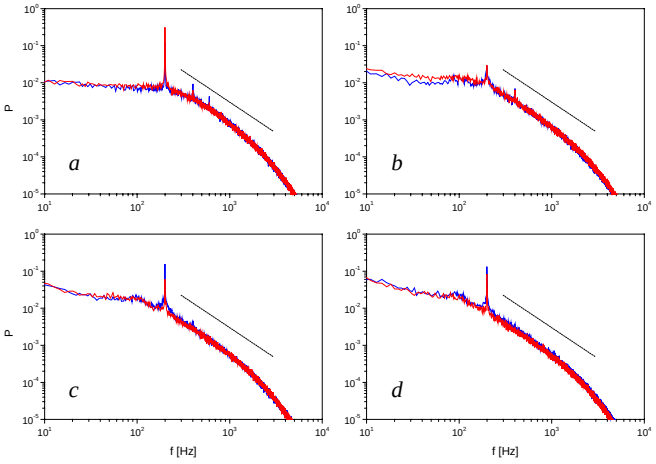

Figure 12. Power spectra of the velocity fluctuations at x/H = 0.5 (*a*), 1.0 (*b*), 1.5 (*c*), and 2.0 (*d*) and $y|_{0.5}$ for the shear layer forced by a single-period actuation (, *St* = 7.36) at the 200 Hz repetition rate and by continuous acoustic actuation (, *St* = 0.74). A slope -5/3 is shown as a reference (---).

between the acoustically- and transitory-forced flows.

Although previous comparison of broadband spectral energy distributions at specific point $y|_{0.5}$ shows virtually no difference between two actuations, it is known that transitory-forced flow results in more diffused coherent structures, and consequently in less spreading and lower TKE levels. Therefore, to elucidate such a difference in spectral analysis, profiles of energy content at coherent motions (f = 200 Hz) are extracted from the derived power spectra at four downstream locations x/H = 0.5, 1, 1.5, and 2. These profiles are shown in Figure 13, along with the corresponding profiles of the baseline (unforced) flow for a reference. At the first measurement location, the biggest enhancement of energy relative to the baseline flow is measured, nearly two orders of magnitude. The shapes of the forced flows are similar to the baseline shape, with the exception of monotone decay of energy towards the low-speed edge in baseline flow and enhancement of energy at the low-speed edge in the forced flows due to the strong entrainment of the surrounding fluid. Two forced profiles are in close agreement, with acoustically-forced profile stronger in the upper and transitory-forced in the lower region of the shear layer. By the next measurement location x/H = 1 (Figure 13*b*), both forced profiles evolve into a double-peak shape. Energy at the coherent motion is most enhanced around the outer edges of the shear layer with suppression in the bulk. It should be noted that zones of most "ampification" of coherent motion in the forced flow correspond to the minimum of the baseline flow and, vice versa, the most energy of the baseline flow is measured in the center of the shear layer where the forced flows exhibit minima. Although the shapes of energy profiles are similar for both actuations, the higher energy content is measured for the acoustically-forced flow. With further evolution and spreading of the flow x/H = 1.5 and 2 (Figures 13*c* and 13*d*, respectively), both forced profiles remain similar, having one dominant peak that develops in the shear layer center and a single minimum. Secondary increase in energy content towards the high-speed edge is still present, but without a distinct peak. General similarity between the forced energy profiles further affirms previous conclusions regarding the similar flow structure in the case of time-harmonic (St = 0.74) and transitory (St = 7.36) flow excitation using the periodic train of vortex pairs.

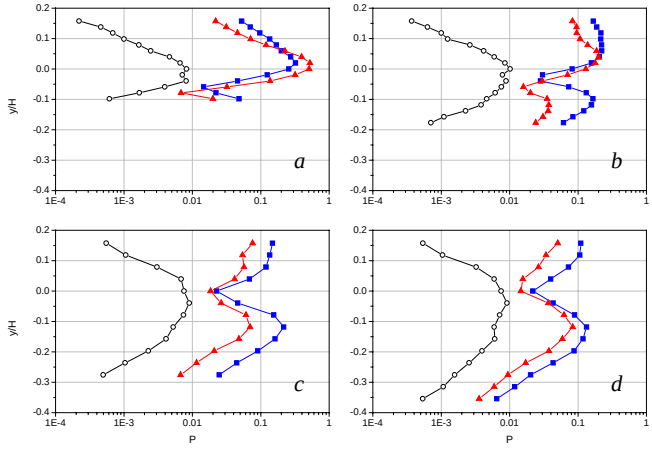

Figure 13. Spectral energy profiles at f = 200 Hz of the flow at x/H = 0.5 (*a*), 1.0 (*b*), 1.5 (*c*), and 2.0 (*d*) for the baseline (∘), continuous acoustic (■, St = 0.74) and a single-period (▲, St = 7.36) actuation at the 200 Hz repetition rate.

V. Burst-Mode Actuation

It was shown before[25] that regardless of the number of continuously injected high-frequency vortex pairs into the upstream boundary layer, any transitory onset of such injection forms a "start-up" large coherent structure due to the transient disruption of vorticity. So far, for the purpose of comparison between the time-harmonic and transitory excitation of the shear layer (Section IV), only a single vortex pair is utilized, thereby accompanying each large coherent structure with a single small-scale vortex, namely CW high-frequency vortex, as schematically shown in Figure 1*c* and measured in Figure 9*a*. By increasing the number of continuously injected vortex pairs at the onset of transitory actuation, an effective burst mode of actuation is applied. Keeping the repetition rate of the burst mode fixed and increasing the number of high-frequency vortex pairs, any single induced coherent structure is accompanied with a train of high-frequency vortices. Thereby, twofold effect on the shear layer is expected: direct small scale manipulation that becomes more prominent with the increase in number of injected vortex pairs, and enhanced large-scale entrainment due to the induced coherent motion. Furthermore, it should be noted that the burst mode transitions to continuous actuation mode in its upper limit. However, there is a remarkable difference in flow dynamics at this limit, as large coherent structure does not form without the transitory onset of actuation, which is absent in the continuous mode. Besides an interest in the effect of different ratios of direct small-scale and indirect large-scale manipulation in the burst mode of actuation, the difference in flow dynamics at transition to pure continuous actuation is another point of motivation of the present study.

Different actuation signals are effected using the 2000 Hz sinusoidal signal modulated with the square wave at the prescribed frequency f = 200 Hz of the coherent structure. Desired number of vortex pairs is injected into the flow by adjustment of the modulation duty cycle. All applied waveforms are schematically shown in Figure 14: a single- (10% duty cycle), three- (30% duty cycle), five- (50% duty cycle), and seven-period (70% duty cycle) transitory actuation. Also, termination point of the burst mode – continuous actuation waveform is applied as well (Figure 14*e*).

The flow structure that corresponds to each of the actuation waveforms shown in Figure 14 is assessed by the phase-averaged PIV measurements and is shown in Figure 15. Raster vorticity plots are shown for the actuation phase (ϕ = 280°) that captures trains of CW vortices. Initial roll-up of the coherent structure is seen in the Figure 15*a* for the case of a single-period actuation, which is analogous in flow structure to Figure 9*a*. Besides the current roll-up, two other coherent structures are visible from the previous transient events. A single CW vortex from the current transient period is already convected ahead of its large-structure pair and interacts with the large coherent structure from the previous actuation period. As CW vortex is injected into the flow, it is convected through the boundary layer and hence moves faster than its large-structure pair, which forms in the low velocity region and thereby is convected at lower speed. Presence of the small-scale CW vortices is more visible in the case of 3-period transitory actuation (Figure 15*b*). The vortices are released such that at this phase the first one already interacts with the previous coherent structure, the second one is between two structures, while the last one interacts with the roll-up of the current coherent structure. As a consequence, the current structure losses some of its coherence and vorticity signature is more diffused. With the increase in number of injected vortex pairs to five (Figure 15*c*) and seven (Figure 15*d*), it is even more clear that a train of CW vortices interacts with the previous coherent structure as well as with the current one, but some of the vortices in the middle align and bridge two consecutive coherent structures, thus remaining in the "braid" region. It seems that partial coalescence of CW vortices is responsible for that as they align themselves. These braids are particularly well formed in the 5- and 7-period actuation. Although the trailing CW vortices act disruptive to coherence of the forming large structure, it appears that the vortices trapped in the braid actually fortify shear layer structure. Finally, with no transitory effect, continuous actuation (Figure 15*e*) generates flow without large-scale structure. There is only a continuous train of CW vortices that is convected along the high-speed edge of the shear layer, and the flow structure in the remaining shear layer is featureless.

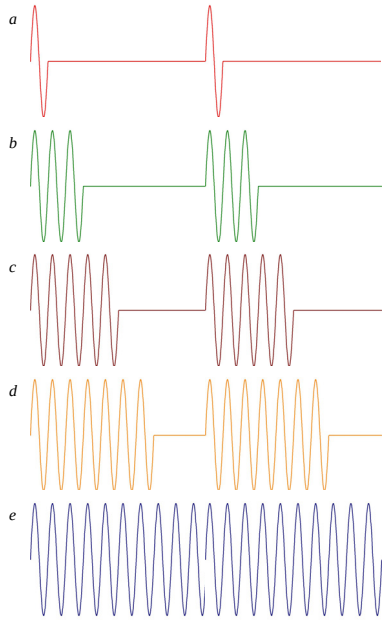

Figure 14. Schematics of the burst high-frequency signal comprised of 1 (*a*), 3 (*b*), 5 (*c*), and 7 (*d*) periods. Continuous signal is shown schematically in (*e*).

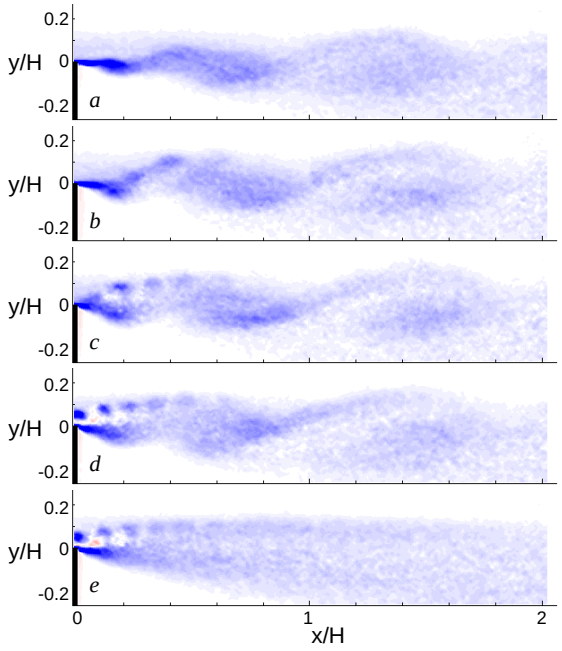

Figure 15. Phase-averaged (ϕ = 280°) raster plots of vorticity for the shear layer forced by the high-frequency (*St* = 7.36) transient 1 (*a*), 3 (*b*), 5 (*c*), and 7(*d*) period signal at the 200 Hz repetition rate, and by the continuous signal (*e*). Vorticity levels are same as in Fig. 3.

After the flow structure is assessed by the phase-averaged PIV measurements, its consequence on the overall flow features is characterized first through the measurements of the mean velocity and TKE fields for all actuation forms that are considered. Raster plots of mean spanwise vorticity with equidistant velocity profiles are shown in Figure 16. The flow actuated by a single-period forcing is shown in Figure 16*a* and corresponds to the transitory case already discussed in Figure 10*b*. It is significant that an increase in number of injected vortex pairs is manifested through the increase in shear layer

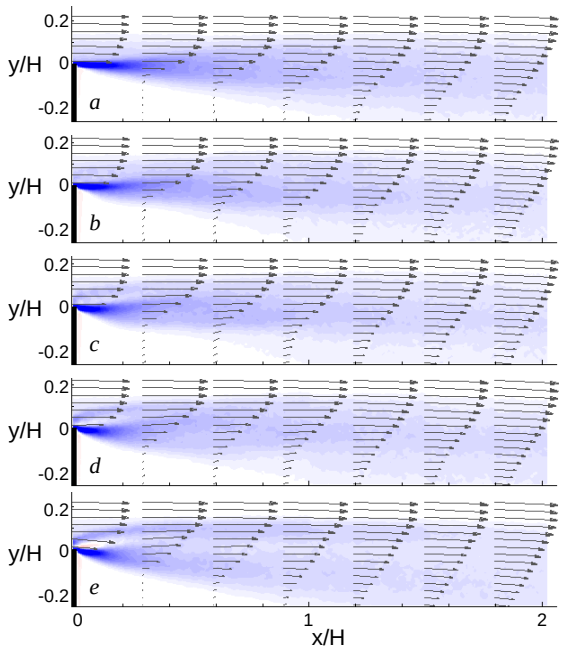

Figure 16. Mean raster plots of vorticity filed with equidistant velocity profiles for the shear layer forced by the high-frequency (*St* = 7.36) transient 1 (*a*), 3 (*b*), 5 (*c*), and 7(*d*) period signal at the 200 Hz repetition rate, and by the continuous signal (*e*). Vorticity levels are same as in Fig. 3.

spreading and faster diffusion of initial zone of high vorticity (e.g., compare Figures 16*a* and 16*c*). These global features also indicate that combined excitation of large scales (that promote entrainment) and small scales (that promote direct mixing) enhances overall mixing and has advantage over a pure enhancement of entrainment. As number of CW vortices is increased to seven (Figure 16*d*), a split in the initial shear layer formation is visible due to the overshooting vortex train. Such split is most dominant for a pure continuous forcing (Figure 16*e*), where a long "shielding" train of high-frequency vortices passes over the shear layer edge. Although in this case there is no significant enhancement of entrainment due to the absence of large-scale excitation, it is remarkable that spreading of the shear layer is even more prominent than in the case of simultaneous large- and small-scale excitation. Such remarkable result is apparently caused by the vectoring effect of the continuous train of vortices, in contrast to the enhanced entrainment due to dynamics of large coherent structures. To further analyze the effect of different ratios of direct small- and large-scale excitation, mean streamwise velocity profiles are plotted in Figure 17 for each of the actuation waveforms at four downstream locations x/H = 0.5, 1, 1.5, and 2. At the first downstream location x/H = 0.5 (Figure 17*a*), a clear trend is visible of increased spreading of the shear layer with the increase in number of injected vortex pairs, including the widest spreading measured for the continuous actuation. At the second downstream location x/H = 1 (Figure 17*b*), 3-, 5-, and 7-period actuations induce similar profiles, while single-period one is noticeably the least spread, and continuous actuation induces the highest spreading. This very same conclusion holds for the other two downstream locations (Figures 17*c* and 17*d*). Such result can be discussed as additional proof that simultaneous large-a and small-scale excitation has advantage over sole manipulation of entrainment, but also as indication that pure high-frequency effect expressed through the flow vectoring can be advantageous over simultaneous actuation of disparate scales.

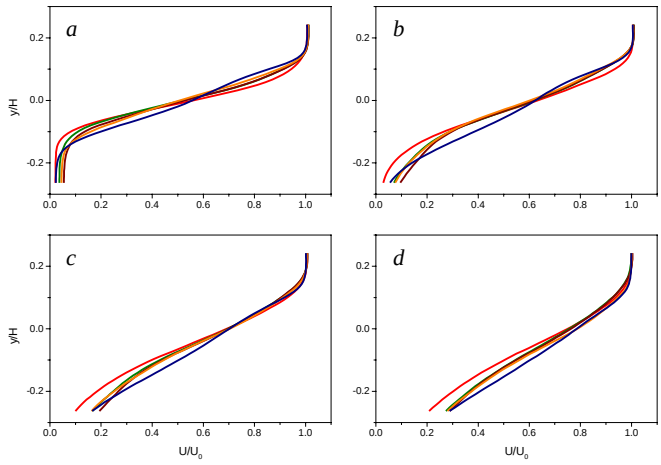

Figure 17. Profiles of the mean *U* velocity component at *x*/*H* = 0.5 (*a*), 1.0 (*b*), 1.5 (*c*), and 2.0 (*d*) for the shear layer forced at *St* = 7.36 by 1 ( ), 3 ( ), 5 ( ), and 7-period ( ) actuation at the 200 Hz repetition rate and by the continuous actuation ( ).

Measured spatial distribution of TKE corresponding to the mean flow fields shown in Figure 17 is plotted in Figure 18. TKE field of the single-period actuation (Figure 18*a*) corresponds to already discussed plot in Figure 10*d*. Zone of high *k* is preceded by formation and initial roll-up of coherent structure, which subsequently transfers energy to small scales. TKE filed of 3-period actuation (Figure 18*b*) shows general increase in *k*-levels relative to the single-period actuation, especially in the shear layer core. Furthermore, immediate interaction region among three CW vortices and large coherent structure is marked by high excursions of TKE. It appears that 5-period actuation (Figure 18*c*) maximizes TKE levels throughout shear layer core. It also becomes evident that the highest TKE zone is formed at the step edge where transitory vortex train starts to create split in the flow with CCW sense of vorticity in between. Domain of the highest TKE near the

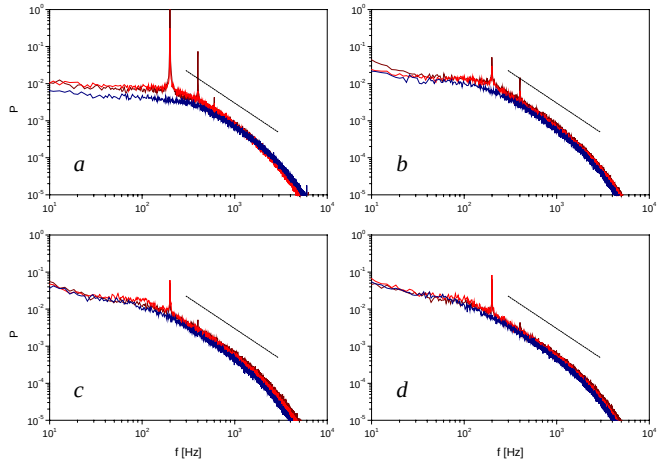

Figure 20. Power spectra of the velocity fluctuations at x/H = 0.5 (*a*), 1.0 (*b*), 1.5 (*c*), and 2.0 (*d*) and $y|_{0.5}$ for the shear layer forced by a single-period ( ), five-period ( ), and continuous ( ) actuation at St = 7.36. A slope -5/3 is shown as a reference (---).

all four transitory actuation scenarios and continuous actuation.

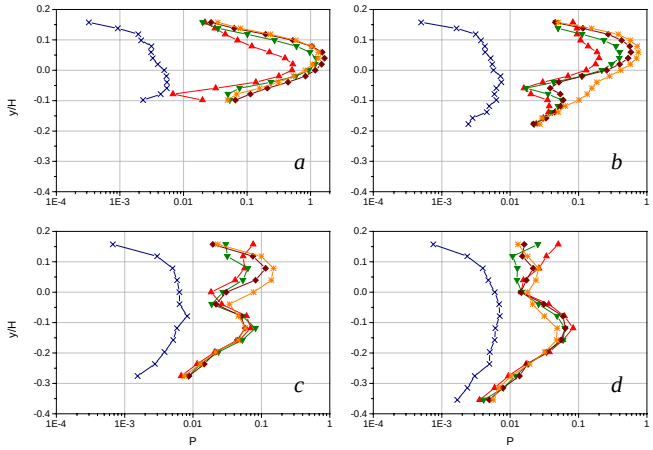

Figure 21. Spectral energy profiles at f = 200 Hz of the flow at x/H = 0.5 (*a*), 1.0 (*b*), 1.5 (*c*), and 2.0 (*d*) for the shear layer forced at St = 7.36 by 1 ( ), 3 ( ), 5 ( ), and 7-period ( ) actuation at the 200 Hz repetition rate and by the continuous actuation ( ).

are present in the flow. Contrary to the transitory actuation, power spectrum of the continuous actuation is featureless as there are no coherent motions in the flow. There is a notable decrease in energy of the large scales in the flow forced by continuous forcing and some increase in energy of the small scales, which is one of the signature features of the direct high-frequency actuation[25]. At second downstream location x/H = 1 (Figure 20*b*), coherent motions are still more prominent in 5-period than in the single-period actuation, while continuous actuation results in spectral energy that is lower across all scales when compared to the other two. At the last two downstream locations x/H = 1.5 and 2 (Figures 20*c* and 20*d*, respectively), spectral energy distributions are commensurate for the 1- and 5-period actuation, while energy of the continuously-forced flow remains lower across all scales.

Finally, profiles of energy content at coherent motion (f = 200 Hz) are plotted in Figure 21 for At the first downstream location x/H = 0.5 (Figure 21*a*), energy content increases with the increase in number of injected vortices, although all cases besides the single-period actuation are closely spaced. All profiles have a single maximum and peak magnitude about two orders of magnitude higher than in the continuously-forced flow where no coherent motions at prescribed frequency f are induced. At the next downstream location x/H = 1 (Figure 21*b*), secondary peak of the energy profile evolves in the shear layer core with still discernable although small increase in energy with an increase in the number of injected vortex pairs. By the next downstream location x/H = 1.5 (Figure 21*c*), energy profiles of transitory actuations have two prominent peaks and a single minima, nearly overlapping in the shear layer core. At the last downstream location x/H = 2 (Figure 21*d*), a strong coincident peak is prominent in all transitory profiles, while increase of energy content towards the high-speed shear layer edge does not form a second maximum anymore.

VI. "Feedback" Suppression

A clear distinction of sole continuous high-frequency actuation is shown in Section V in terms of diminished levels of turbulent kinetic energy, which is attributed to its strong dissipative effect in the localized zone of injection. Next step is to extend such stabilizing effect of continuous actuation to the flow with independently-driven excitation of large coherent structures. The flow configuration is shown in Figure 22*a*, where the shear layer feedback is emulated by pressure fluctuations that are induced by an acoustic speaker (at the bottom of the backward-facing step, as already discussed in Sections II and IV). The shear layer having a "natural", unstable frequency of f_n = 243, (St_θ = 0.032) is subjected to a "feedback" frequency f_s = 180 Hz. The "feedback-forced" flow is characterized by phase-averaged (relative to f_s) PIV measurements of the cross stream velocity component $V_C(\phi)$

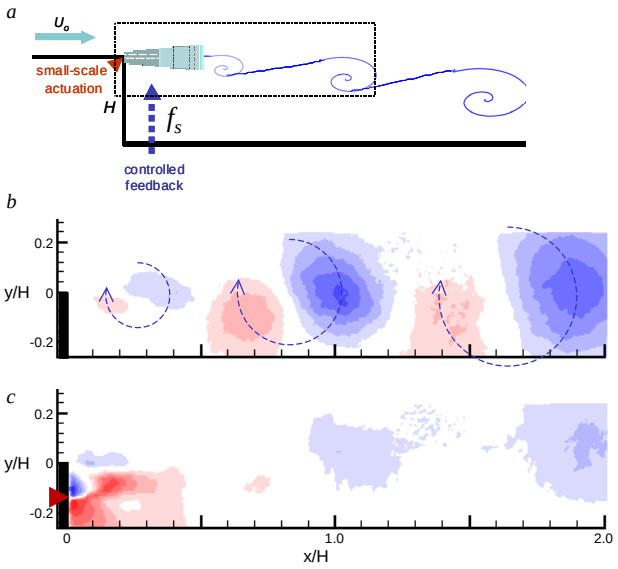

Figure 22. Stabilization of a shear layer driven by external acoustic "feedback" at f_s = 180 Hz: *a*) Flow configuration and contours of the phase-averaged cross stream velocity $V_C(\phi)$ in the absence (*b*) and presence (*c*) of dissipative actuation (f = 2000 Hz).

(Figure 22*b*) and shows three successive coherent structures induced within the field of view. Next, the *same* flow is controlled using dissipative, continuous high-frequency actuation at $f = 2000$ Hz and the resulting phase-averaged flow filed is shown in Figure 22*c* (the red triangle marks the position of the high-frequency actuators). As a result of the dissipative actuation, the feedback-induced, phase-locked flow structures are almost completely suppressed indicating that induced instabilities are no longer amplified by the modified base flow.

VII. Conclusions

Transitory control of a plane shear layer is effected by pulse actuation where the period of a single pulse is considerably shorter than the unstable period of the baseline flow. In the present experiments the pulse actuation is repeated time-periodically and the duty cycle of the intermittent pulse trains is varied between single pulse and continuous actuation. The ensuing flow fields are analyzed using high-resolution PIV and hot-wire measurements. It is shown that the onset of a single transitory actuation pulse induces a roll-up of a discrete large-scale coherent vortical structure by the transient disruption (and subsequent roll up) of the vorticity layer. The pulse actuation is effected by the generation of small-scale counter-rotating vortex pairs that interact with the base flow. While it is shown that the evolution of the flow is almost identical when it is forced by time-periodic pulse actuation and continuous time harmonic actuation (at the same frequency) by an external acoustic source, the coherence of the large-scale structures in transitory actuation is somewhat diminished. This loss of coherence can be attributed to the interaction between the large vortex (during its roll up) with the actuation (small-scale) vortex.

Although a large-scale vortical structure is formed by the actuation of a *single* pulse, actuation with an intermittent train of such pulses (burst mode) results in the interaction of the large vortex with a train of high-frequency vortices. Thereby, twofold effect on the shear layer is imposed: direct small scale manipulation due to the injected vortex pairs, and enhanced large-scale entrainment by the induced coherent motion. The upper limit of the burst mode is continuous (high-frequency) actuation. At this limit, there is no transitory formation of large-scale coherent motions. Analysis of instantaneous and mean flow fields of different burst-mode actuations indicates that combined actuation of large scales (that promote entrainment) and small scales (that promote direct mixing) enhances overall mixing and has advantage over enhancement of entrainment only. It is shown that continuous pulse actuation generates only a continuous train of vortices, which are convected along the high-speed edge of the shear layer, and the flow structure in the remaining shear layer is essentially featureless. Nonetheless, it is remarkable that spreading of the shear layer under continuous high-frequency pulse train is even more prominent than in the case of simultaneous large- and small-scale excitation. This is apparently the result of flow vectoring induced by the continuous train of actuation vortices, unlike due to entrainment effected by the large vortical structures. These findings indicate that simultaneous actuation of small- and large-scales can lead to better overall mixing compared to large-scale actuation only. It is noteworthy that the flow vectoring induced by continuous high frequency actuation can lead to better shear layer spreading than in the presence of the large scale structures.

Finally, the present experiments have also demonstrated that the high frequency actuation in the presence of external acoustic disturbances can substantially diminish the receptivity of the baseline flow to these disturbances. The present experiments emulate the presence of acoustic feedback and show that high-frequency actuation prevents the formation of the large coherent structures in the near field of the flow.

References

[1]Brown, G. L. and Roshko, A., "On Density Effects and Large Structure in Turbulent Mixing Layers," *J. Fluid Mech.*, **64**, 1974, pp. 775–816.

[2]Winant, C. D. and Browand, F. K., "Vortex Pairing, the Mechanism of Turbulent Mixing Layer Growth at Moderate Reynolds Number," *J. Fluid Mech.*, **63**, 1974, pp. 237-255.

[3]Ho, C-M. and Huerre, P., "Perturbed Free Shear Layers", *Ann. Rev. Fluid Mech.*, **16**, 1984, pp. 365-424.

[4]Roberts, F.A. and Roshko, A. "Effects of Periodic Forcing on Mixing in Turbulent Shear Layers and Wakes", *AIAA Paper* 85-0570, 1985.

[5]Breidenthal, R. E. "Response of Plane Shear Layer and Wakes to Strong Three-Dimensional Disturbances," *Phys. Fluids*, **23**, 1980, pp. 1929-1932.

[6]Nygaard, K. J. & Glezer, A. "Evolution of Streamwise Vortices and Generation of Small-scale Motion in a Plane Shear Layer," *J. Fluid Mech.* **231**, 1991, 257-301.

[7]Ho, C-M. and Huang, L-S., "Subharmonics and Vortex Merging in Mixing Layers", *J. Fluid Mech*., **119**, 1982, pp. 443-473.

[8]Oster, D. and Wygnanski, I., "The Forced Mixing Layer Between Parallel Streams", *J. Fluid Mech*., **123**, 1982, pp. 91-130.

[9]Reisenthel, P. H., Nagib, H. M., and Koga, D. J., "Control of Separated Flows Using Forced Unsteadiness," *AIAA Paper* 85-0556, 1985.

[10]Vandsburger, U. and Ding, C., "Self-excited Wire Method for the Control of Turbulent Mixing Layers", *AIAA J.* **33**, 1995, pp. 1032-1037.

[11]Huang, L.-S. and Ho, C.-M., "Small-Scale Transition in a Plane Mixing Layer," *J. Fluid Mech.*, **210**, 1990, pp. 475–500.

[12]Ho, C.-M., Zohar, Y., Foss, J. K., and Buell, J. C., "Phase Decorrelation of Coherent Structures in a Free Shear Layer," *J. Fluid Mech.*, **230**, 1991, pp. 319–337.

[13]Chun, K. B. and Sung, H. J., "Control of Turbulent Separated Flow over a Backward-facing Step by Local Forcing," *Exp. Fluids*, **21**, 1996, pp. 417–426.

[14]Chun, K. B., Lee, I., and Sung, H. J., "Effect of Spanwise-Varying Local Forcing on Turbulent Separated Flow over a Backward-Facing Step," *Exp. Fluids*, **26**, 1999, pp. 437–440.

[15]Kaiktsis, L. and Monkewitz, P. A., "Global Destabilization of Flow over a Backward-Facing Step," *Phys. Fluids*, **15**, 2003, pp. 3647–3658.

[16]Amitay, M., Honohan, A.M., Trautman, M., and Glezer, A., "Modification of the Aerodynamic Characteristics of Bluff Bodies Using Fluidic Actuators", *AIAA Paper* 97-2004, 1997.

[17]Honohan, A.M., Amitay, M., and Glezer, A., "Aerodynamic Control Using Synthetic Jets", *AIAA Paper* 2000-2401, 2000.

[18]Wiltse, J.M. and Glezer, A., "Manipulation of Free Shear Flows using Piezoelectric Actuators", *J. Fluid Mech*., **249**, 1993, pp. 261-285.

[19]Wiltse, J.M. and Glezer, A., "Direct Excitation of Small-scale Motions in Free Shear Flows", *Phys. Fluids*, **10**, 1998, pp. 2026-2036.

[20]Smith, B.L. and Glezer, A. "Jet Vectoring using Synthetic Jets", *J. Fluid Mech*., **458**, 2002, pp. 1-34.

[21]Davis, S.A. and Glezer, A., "The Manipulation of Large- and Small-Scales in Coaxial Jets Using Synthetic Jet Actuators", *AIAA Paper* 2000-0403, 2000.

[22]Smith, B.L. and Glezer, A., "The Formation and Evolution of Synthetic Jets", *Phys. Fluids*, **10**, 1998, pp. 2281-2297.

[23]Glezer, A. and Amitay, M., "Synthetic Jets", *Annu. Rev. Fluid Mech*., **34**, 2002, pp. 503-529.

[24]Vukasinovic, B., Lucas, D. G., and Glezer, A., "Direct Manipulation of Small-Scale Motions in a Plane Shear Layer", *AIAA Paper* 2004-2617, 2004.

[25]Vukasinovic, B., Lucas, D. G., and Glezer, A., "Controlled Manipulation of Small- and Large- Scales in a Turbulent Shear Layer, Part I: Experimental Studies", *AIAA Paper* 2005-4753, 2005.

[26]Funk, R., Parekh, D., Crittenden, T., and Glezer, A., "Transient Separation Control Using Pulse Actuation", *AIAA Paper* 2002-3166, 2002.

[27]Brzozowski, D., and Glezer, A., "Transient Separation Control Using Pulse- Combustion Actuation", *AIAA Paper* 2006-3024, 2006.